

Potential Stibnite Reference Materials for in situ S and Sb Isotope measurement by LA-MC-ICP-MS

Jiaxin Zhang,^a Kejun Hou,^{a,*} Ran Wang,^a Yutian He,^{a,b} Tao Yang,^b Xiaowei Gao,^{a,c} and Mengqi Zhang^{a,c}

^aMNR Key Laboratory of Metallogeny and Mineral Assessment, Institute of Mineral Resources, Chinese Academy of Geological Sciences, Beijing 100037, P. R. China

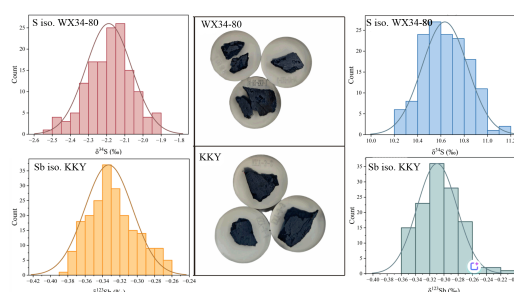
^bFaculty of Land Resources Engineering, Kunming University of Science and Technology, Kunming 650093, P. R. China

^cChina University of Geosciences, Beijing 100083, P. R. China

Received: February 09, 2026; Revised: March 17, 2026; Accepted: March 17, 2026; Available online: March 18, 2026.

DOI: 10.46770/AS.2026.027

ABSTRACT: Stibnite is the principal sulfide mineral and the most important ore mineral in antimony deposits worldwide. In situ S and Sb isotope analyses of stibnite are crucial for investigating the genesis of antimony deposits and for deciphering detailed mineralization processes. To obtain reliable in-situ isotopic data, matrix-matched reference materials are essential for correcting instrumental mass fractionation. In this study, two natural stibnite samples (WX34-80 and KKY) were characterized on the basis of their elemental and isotopic compositions. The results demonstrate that both samples are homogeneous in terms of S and Sb contents, as well as their isotopic signatures, and exhibit significantly distinct sulfur isotopic compositions, rendering them highly suitable reference standards for in situ Sb and S isotope analyse using LA-MC-ICP-MS. Based on IRMS measurements, the recommended $\delta^{34}\text{S}_{\text{V-CDT}}$ values are $-2.17 \pm 0.29\text{‰}$ (2SD, $n = 18$) for WX34-80 and $10.63 \pm 0.38\text{‰}$ (2SD, $n = 18$) for KKY. Correspondingly, SN-MC-ICP-MS analyses yield recommended $\delta^{123}\text{Sb}_{\text{Spex}}$ values of $-0.33 \pm 0.07\text{‰}$ (2SD, $n = 8$) for WX34-80 and $-0.29 \pm 0.05\text{‰}$ (2SD, $n = 8$) for KKY.



INTRODUCTION

With the expansion of emerging industries and advancements of advanced manufacturing, antimony has emerged as a strategically critical emerging mineral resource.¹⁻³ Stibnite is the primary—and frequently the sole—antimony-bearing mineral in antimony deposits.⁴⁻⁸ Accordingly, investigating the geochemical characteristics of stibnite, particularly through combined sulfur (S) and antimony (Sb) isotope analyses, provides robust constraints for tracing the sources of ore-forming materials, reconstructing fluid evolution processes, and deciphering mineralization mechanisms.^{9,10}

Traditional methods for analyzing sulfur and antimony isotopes in stibnite predominantly rely on bulk-rock analysis. To determine the sulfur isotope composition, gas stable isotope ratio mass spectrometry (GS-IRMS) is commonly employed: single stibnite mineral samples are ground, mixed with CuO in a fixed proportion,

and heated to high temperatures to oxidize sulfur to SO_2 .^{6,11-16} The sulfur isotope composition is then measured using gas isotope mass spectrometry, achieving an analytical precision better than $\pm 0.2\text{‰}$.^{11,15} Antimony isotope analysis is primarily conducted using solution-based multi-collector inductively coupled plasma mass spectrometry (MC-ICP-MS). Following sample digestion and resin-based separation/purification, isotopic compositions are determined by MC-ICP-MS, with precision typically better than 0.04‰ (2SD).¹⁷⁻²⁷ Although this bulk-sample approach yields high-precision and high-accuracy isotopic data, it involves complex sample preparation, consumes significant chemical reagents, and ultimately provides averaged whole-rock isotopic values.²⁸⁻³⁴ These results do not capture the microscale isotopic heterogeneity, thus limiting their integration with petrographic observations to elucidate detailed metallogenic processes of stibnite.³⁵

In recent years, micro-scale analytical techniques, particularly

laser ablation multi-collector inductively coupled plasma mass spectrometry (LA-MC-ICP-MS), have become a forefront area in isotope geochemistry due to their high spatial resolution, precision, efficiency, and environmentally friendly analytical processes.^{32,36-38} Dai *et al.*³³ established an analytical method for in situ sulfur isotope analysis of stibnite using ns-LA-MC-ICP-MS; Kaufmann *et al.*³⁹ and Wang *et al.*³⁴ developed analytical methods for in situ determination of stable Sb isotope compositions in stibnite using fs-LA-MC-ICP-MS. Most of these in situ measurements used standard-sample bracketing to correct for mass bias. Therefore, the development of high-quality natural stibnite reference materials is essential for reliable microscale S and Sb isotope analyses. Currently, only a handful of stibnite reference materials, including natural minerals and synthesized solid minerals, are available for in situ S and Sb isotope analyses. The natural stibnite reference material BJ-Snt ($\delta^{34}\text{S} = -0.71 \pm 0.32\text{‰}$) and the in-house stibnite ultra-fine pressed powder pellet YS14 developed by Dai *et al.*³³ are available for in-situ sulfur isotope microanalysis. Kaufmann *et al.*³⁹ prepared the stibnite reference material SC (stibnite powder melted at 650 °C for 2 days, and cool down slowly in the furnace, $\delta^{123}\text{Sb} = -0.189 \pm 0.031\text{‰}$), and conducted a homogeneity assessment of Sb isotopes using a commercial EMP analysis standard. Wang *et al.*³⁴ developed two natural stibnite reference materials, DC ($\delta^{123}\text{Sb} = 0.02 \pm 0.04\text{‰}$) and BJS ($\delta^{123}\text{Sb} = -0.37 \pm 0.05\text{‰}$), as microanalytical reference materials for in situ Sb isotope analysis.

Matrix effects during analysis remain a major challenge to measurement accuracy of LA-MC-ICP-MS.^{33,40} While the adoption of femtosecond laser ablation systems and reactive matrices with water vapor introduction can substantially reduce or even eliminate such effects,^{41,42} the use of matrix-matched reference materials for fractionation correction continues to be the most reliable approach to mitigating matrix interference.⁴³ Furthermore, reference materials serve as a crucial foundation for method validation, quality control, and the comparison of data across different laboratories.^{44,45} Given the rapid development of microanalytical techniques, which continuously consume high-quality reference materials, and the current scarcity of available standards, it is imperative to develop new natural stibnite standard materials for in situ S and Sb isotope analyses by LA-MC-ICP-MS.

In this study, we characterized two natural stibnite samples, WX34-80 and KKY, as potential reference materials for in situ sulfur and antimony isotope analyses. Extensive data indicate that these samples exhibit consistent chemical characteristics, including sulfur and antimony homogeneity and simple elemental compositions. We also conducted supplementary determinations of S and Sb isotope composition for existing stibnite reference materials.

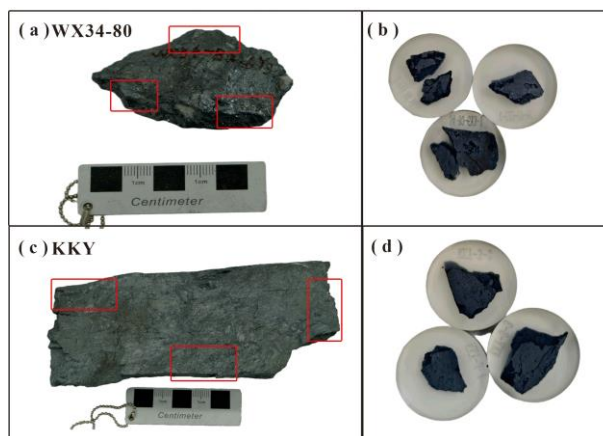


Fig. 1 Hand specimens of stibnite samples WX34-80 and KKY. The red borders mark the locations from which fragments were taken for analysis. (a) Sample WX34-80 from the Woxi Au-Sb-W deposit, Hunan; (c) Sample KKY from the Zhazixi Sb-W deposit, Hunan; (b, d) representative fragments mounted in epoxy.

EXPERIMENTAL

Sample description and preparation. Two natural stibnite samples used in this study, designated WX34-80 and KKY, were collected from the Xiangzhong metallogenic province. Sample WX34-80 (Fig. 1a–b) originated from the Woxi Au-Sb-W deposit, one of the largest layered, sediment-hosted polymetallic deposits in the Jiangnan metallogenic belt of the South China Block, and represents a typical Au-Sb-W mineralization style in this orogenic setting. All orebodies occur in the footwall of the Woxi Deep Fault.⁴⁶⁻⁴⁸ Sample KKY (Fig. 1c–d) was collected from the Zhazixi Sb-W deposit, situated in the middle segment of the Xuefeng Arcuate Tectonic Belt, which represents a typical vein-type Sb deposit in China.⁴⁹ For analysis, three distinct locations within each sample were selected. Subsamples from these locations were mounted in 2.5 cm diameter epoxy resin mounts, polished with diamond paste, and ultrasonically cleaned in ultrapure water to obtain flat surfaces suitable for EPMA and in situ S–Sb isotope analyses. Additionally, some stibnite fragments were ground into powder and immediately transferred into clean sample bags for subsequent bulk S and Sb isotope analyses by IRMS and SN-MC-ICP-MS, respectively.

The standard reference material BJ-Snt for sulfur isotope analysis from Dai *et al.* (2023),³³ was obtained from the Baiji Pb–Zn–Sb ore deposit located in Weixi County, western Yunnan Province, China. The standard reference materials DC and BJS for antimony isotope analysis from Wang *et al.*³⁴ were selected from the Dachang tin polymetallic deposit in Guangxi and the Bijiashan stibnite deposit in Yunnan, respectively.

Analytical techniques

Electron probe microanalysis (EPMA). Mineral compositions were determined at the MNR Key Laboratory of Metallogeny and Mineral Assessment, Institute of Mineral Resources, Chinese Academy of Geological Sciences, using a JEOL JXA-8230 Electron Probe Micro Analyzer (EPMA) equipped with four wavelength-dispersive spectrometers. The samples were firstly coated with a ca. 20 nm thin conductive carbon film prior to analysis. The details of the EPMA method were described by Yang *et al.* (2022).⁵⁰ During the analysis, an accelerating voltage of 15 kV, a beam current of 20 nA and a 5 μm spot size were used for mineral analysis. Natural minerals and synthetic oxides were used as standards. Data were corrected on-line using a modified ZAF (atomic number, absorption, fluorescence) correction procedure.

LA-ICP-MS. The stibnite trace element analyses were conducted using a RESolution S-155 laser ablation system (Applied Spectra Inc., Sacramento, CA, USA) coupled with an Element XR ICP-MS instrument (Thermo Fisher, USA) at the MNR Key Laboratory of Metallogeny and Mineral Assessment, Institute of Mineral Resources, CAGS (IMR, CAGS). Ablation was performed using He–Ar mixture. Each spot analysis consisted of a 2 s pre-ablation, approximately 20 s of background acquisition and approximately 40 s of sample data acquisition. The analyses were conducted using a 30 μm spot diameter, a 6 Hz frequency and a 5 J cm^{-2} energy density. Detailed operating conditions for the laser ablation system and ICP-MS instrument are listed in Table 1. SRM 610 glass and MASS-1 were used as external standards, and the concentrations of elements were calculated using

ICPMSDataCal 10.8⁵¹ and calibrated using multiple external standards without an internal standard. Repeated analyses consistently demonstrated precision and accuracy better than 10% for most analyzed elements.

Isotope ratio mass spectrometry (IRMS). Bulk stibnite sulfur isotope analysis in this study was conducted at the MNR Key Laboratory of Metallogeny and Mineral Assessment, Institute of Mineral Resources, CAGS (IMR), the Analytical Laboratory of the Beijing Research Institute of Uranium Geology (BRIUG) and the Beijing Createch Testing Technology Co., Ltd (Createch). Sulfur isotope measurements were conducted by the coupling a MAT 253 (IMR, CAGS; Createch) and Delta V Plus (BRIUG) Gas Isotope Mass Spectrometer with a Flash 2000 Elemental Analyzer, all manufactured by Thermo Fisher Scientific. Stibnite powder samples were wrapped in tin capsules and introduced into the elemental analyzer through an AS200 auto-sampler for SO_2 generation. The operating parameters of the elemental analyzer were listed in Table 1. International Atomic Energy Agency (IAEA) reference materials IAEA-S-1, IAEA-S-2 and IAEA-S-3 were used as standard. All data were expressed relative to the international sulfur isotope standard V-CDT, and the calibrated values of the samples were obtained via linear calibration against the above three reference materials, with analytical precision better than $\pm 0.2\%$ (2SD).^{45,52}

Solution MC-ICP-MS. Sb isotope compositions were measured using a Thermo Scientific Neptune Plus MC-ICP-MS at the Institute of Mineral Resources, CAGS and the China University of Geosciences (CUG). Approximately 50 mg of each sample was

Table 1. Operating conditions for IRMS and LA-MC-ICP-MS

Instrument	Parameter setting
IRMS	
Mass Spectrometer	IMR, CAGS Createch: MAT 253; BRIUG: Delta V Plus
Elemental Analyzer	Flash 2000
Carrier gas flow rate (He)	0.1 L/min
Oxygen flow rate	0.15 L/min
Reaction furnace temperature	1020 °C
Chromatographic column temperature	90 °C
Pressure of He in the ConFlo IV interface	1.01×10^5 Pa
Ion current intensity	2.5 V
LA-MC-ICP-MS	
Laser model	Resolution S155
Energy density	5 J cm^{-2}
Frequency	5 Hz
Beam spot diameter	30 μm
Carrier gas flow rate	~0.6 L/min
Wavelength	193nm
MC-ICP-MS model	Neptune Plus
Sample gas (Ar)	~1.0L/min
Auxiliary gas (Ar)	~0.6 L/min
Cooling gas (Ar)	~15.0L/min
Faraday cup structure	C- ³² S, H2- ³⁴ S; C- ¹²¹ Sb, H2- ¹²³ Sb
Mass resolution	Medium resolution for S and Low resolution for Sb
Integral time	Background time: 20 seconds, erosion time: 40 seconds

dissolved in 5 mL of ultra-pure aqueous solution overnight. The complete dissolution of the samples was visually confirmed. Samples were diluted more than 100,000 times in a 0.5 M nitric acid solution containing trace HF (0.01 M) so that Sn remained in solution. The samples did not require ion exchange chromatography, as reported in previous studies.^{20,22,53} Solutions were measured in low resolution mode. Peak background measurements were subtracted for each analysis and the samples were matched within 10% of the standard voltages. Background Sb isotope voltages were no greater than 3 mV for each measured mass. Mass bias was corrected using the standard-sample-standard bracketing method, and all samples were calibrated using Spex Sb standard (USA, lot: CL 10-49SBY, $\delta^{123}\text{Sb}$ values of standard solutions Spex relative to NIST SRM 3102a were $0.29 \pm 0.03\%$).⁵⁴ The measurements were repeated three times and 30 ratios were measured in each cycle.

LA-MC-ICP-MS. In situ S and Sb isotope analyses were also performed at the Key Laboratory of Metallogeny and Resource Assessment, Ministry of Natural Resources, Institute of Mineral Resources, Chinese Academy of Geological Sciences, China. Measurements were performed using a Neptune Plus MC-ICP-MS (Thermo Fisher Scientific, Bremen, Germany) coupled with a RESolution-LR-S155 laser ablation system (ASI, USA). The laser system was equipped with a 193 nm ArF excimer laser, two-volume ablation cell, computer-controlled operation, and high-precision X–Y translation stage. Helium was used as the carrier gas at a flow rate of 600 mL min⁻¹ and was mixed with argon make-up gas inside the ablation cell. The resulting aerosol was transported directly through the gas mixture into the ICP. Analyses were conducted in single-spot ablation mode using a 30 μm spot size, a 5 Hz repetition rate, and a constant laser fluence of 5 J·cm⁻².

During the in situ sulfur isotope analysis, a minimum signal intensity of 10 V was maintained to ensure optimal signal stability and analytical precision. The specific instrumental parameters are listed in Table 1. The Neptune Plus MC-ICP-MS was equipped with nine Faraday cups and 10¹¹ Ω resistor amplifiers. Operating in medium-mass-resolution mode (approximately 7000), the instrument effectively resolved sulfur isotopes from potential isobaric and polyatomic interferences (e.g., ¹⁶O–¹⁶O and ¹⁵N–¹⁶O–¹H for ³²S; ¹⁶O–¹⁸O, ¹⁷O–¹⁶O–¹H, and ³³S–¹H for ³⁴S). Sulfur isotopes (³²S and ³⁴S) were collected simultaneously in static mode using the C and H2 Faraday cups, respectively. Instrumental mass bias was corrected using a standard–sample–bracketing (SSB) protocol, with reference materials analyzed before and after every three samples.

The measured ³⁴S/³²S ratios were conveniently converted to per mil variation relative to V-CDT:

$$\delta^{34}\text{S}_{\text{V-CDT}}(\text{‰}) = [({}^{34}\text{S}/{}^{32}\text{S})_{\text{sample}}/({}^{34}\text{S}/{}^{32}\text{S})_{\text{V-CDT}} - 1] \times 1000 \quad (1)$$

The published reference material BJ-Snt ($\delta^{34}\text{S} = -0.71 \pm 0.32\%$) was employed for mass bias correction. Repeated measurements of ZZX yielded a $\delta^{34}\text{Sb}$ value of $10.39 \pm 0.36\%$ (2SD, n = 30), which is in good agreement with the recommended value of $10.45 \pm 0.62\%$ (2SD).³³

In situ Sb isotope were obtained using LA-MC-ICP-MS. The signals of the Sb isotopes ¹²¹Sb and ¹²³Sb were simultaneously and statically collected using C and H2 Faraday cups, respectively, in static collection mode, operating in low mass resolution mode. Detailed instrument settings and operational parameters are summarized in Table 1, signal intensity of approximately 20 V on ¹²³Sb was achieved at 30 μm spot size. The isotopic composition of antimony was conveniently converted to per mil variation relative to Spex:

$$\delta^{123}\text{Sb} = [({}^{123}\text{Sb}/{}^{121}\text{Sb})_{\text{sample}}/({}^{123}\text{Sb}/{}^{121}\text{Sb})_{\text{Spex}} - 1] \times 1000 \quad (2)$$

The standard reference materials DC ($\delta^{123}\text{Sb} = 0.02 \pm 0.04\%$) was employed for mass bias correction. Repeated measurements of BJS yielded a $\delta^{123}\text{Sb}$ value of $-0.34 \pm 0.05\%$ (2SD, n = 30), which is in good agreement with the recommended value $-0.37 \pm 0.05\%$ (2SD).³⁴

RESULTS AND DISCUSSION

Major and trace element. A total of 34 random spot analyses were conducted on WX34-80 and KKY using EPMA and LA-ICP-MS. For WX34-80, the average S and Sb contents ranged from 27.18 wt% to 28.57 wt% and from 71.31 wt% to 72.23 wt%, respectively (Table S1). Similarly, the contents of S and Sb in KKY ranged from 27.23 wt% to 28.43 wt%, and from 70.67 wt% to 71.85 wt%, respectively (Table S1). These two sample matrices exhibited relatively simple compositions. Beyond the primary constituents S and Sb, samples contain only trace elements (e.g., Si, Cu, As, Pb, and Cl) at concentrations ranging from tens to hundreds of ppm (Table S1). These results indicated a high degree of chemical homogeneity between WX34-80 and KKY. Importantly, the samples were virtually free of elements such as Sn and Te, which could otherwise interfere with the determination of Sb. This is because the isotope ¹²³Te can cause isobaric interference with ¹²³Sb.³⁹ The hydrides of tin (¹²⁰Sn–H and ¹²²Sn–H) interfered with both ¹²¹Sb and ¹²³Sb during the analysis. Previous studies^{55,56} showed that the interference could be neglected when the Te/Sb and Sn/Sb concentration ratios were lower than 0.01 and 0.1; however, Te concentrations were below the detection limit of ICP-MS and the highest Sn concentration observed in the analyzed stibnite samples was 1.86 ppm, which was insufficient to induce a significant effect.

IRMS S isotope measurement. Sulfur isotope analysis was performed on 18 fragments from samples WX34-80 and KKY using

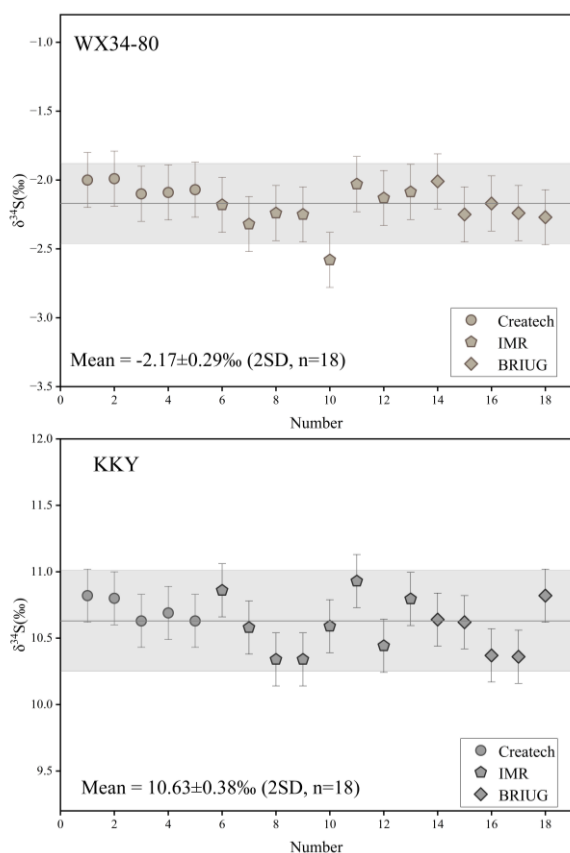


Fig. 2 $\delta^{34}\text{S}$ values of WX34-80 and KKY. Error bars are determined by repeated measurements of reference materials as the unknown samples. 'IMR' represent Institute of Mineral Resources, Chinese Academy of Geological Sciences; 'BRIUG' represent Beijing Research Institute of Uranium Geology; 'Createch' represent Beijing Createch Testing Technology Co., Ltd.

IRMS in three independent laboratories (Fig. 2). For WX34-80, $\delta^{34}\text{S}$ values ranged from -2.58‰ to -1.99‰ , with an average of $-2.17 \pm 0.29\text{‰}$ (2SD, $n = 18$). For KKY, $\delta^{34}\text{S}$ values ranged from 10.34‰ to 10.93‰ , yielding an average of $10.63 \pm 0.38\text{‰}$ (2SD, $n = 18$). The results obtained from these three laboratories showed a high degree of consistency.

Solution MC-ICP-MS Sb isotope measurement. Eight sample fragments from each stibnite specimen, WX34-80 and KKY, were analyzed for Sb isotopes using the SN-MC-ICP-MS method at two independent laboratories (Fig. 3). The results from both laboratories were consistent within analytical uncertainty. The $\delta^{123}\text{Sb}$ values of WX34-80 ranged from -0.37‰ to -0.27‰ , with an average of $-0.33 \pm 0.07\text{‰}$ (2SD, $n = 8$). For KKY, the $\delta^{123}\text{Sb}$ values vary between -0.30‰ to -0.24‰ , yielding an average of $-0.29 \pm 0.05\text{‰}$ (2SD, $n = 8$). In addition, the published reference material BJ-Snt was analyzed by SN-MC-ICP-MS in this study, yielding a $\delta^{123}\text{Sb}$ value of $0.14 \pm 0.05\text{‰}$ (2SD, $n = 2$).

Homogeneity assessment. Homogeneity is a fundamental

requirement for any reference material.^{57,58} The homogeneity of sulfur and antimony in WX34-80 and KKY was evaluated using LA-MC-ICP-MS.

LA-MC-ICP-MS S isotope measurement. In situ sulfur isotope analysis was performed on the sample mounts using a non-selective, random spot selection method. A total of 144 in situ sulfur isotope analyses were conducted on sample WX34-80. Among these, 74, 35, and 35 analytical spots were obtained from mount 1, mount 2, and mount 3, yielding average $\delta^{34}\text{S}$ values of $-2.21 \pm 0.27\text{‰}$ (2SD, $n = 74$), $-2.10 \pm 0.15\text{‰}$ (2SD, $n = 35$), and $-2.23 \pm 0.21\text{‰}$ (2SD, $n = 35$), respectively, and yielding an average $\delta^{34}\text{S}$ value of $-2.19 \pm 0.25\text{‰}$ (2SD, $n = 144$) (Fig. 4a–b). For sample KKY, 144 in situ sulfur isotope analyses were performed. The spots were distributed as, 53, 56, and 35 across mount 1, mount 2, and mount 3, with corresponding average $\delta^{34}\text{S}$ values of $10.73 \pm 0.37\text{‰}$ (2SD, $n = 53$), $10.54 \pm 0.34\text{‰}$ (2SD, $n = 56$), and $10.63 \pm 0.35\text{‰}$ (2SD, $n = 35$), respectively, yielding an average $\delta^{34}\text{S}$ value of $10.63 \pm 0.39\text{‰}$ (2SD, $n = 144$) (Fig. 4c–d). The mean $\delta^{34}\text{S}$ values obtained from in situ analysis were consistent with those derived from IRMS ($-2.17 \pm 0.29\text{‰}$ for WX34-80 and $10.63 \pm 0.38\text{‰}$ for KKY) within the 2SD analytical uncertainty.

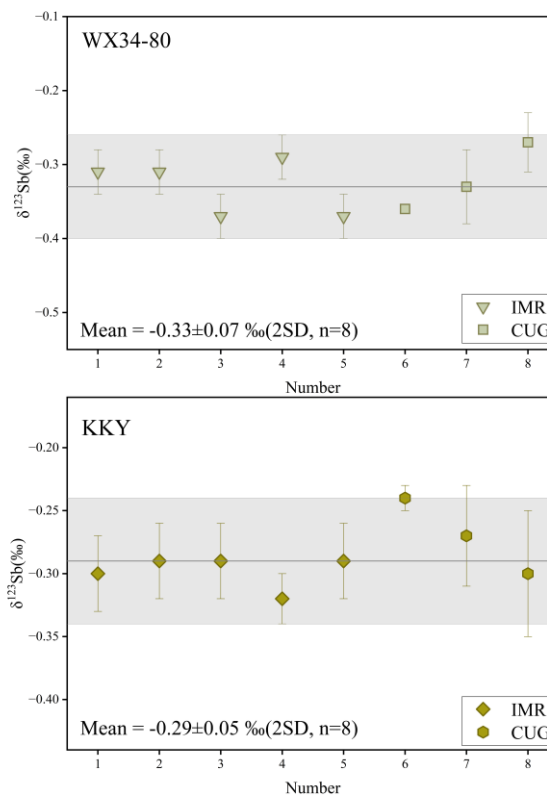


Fig. 3 $\delta^{123}\text{Sb}$ values of WX34-80 and KKY. Error bars are determined by repeated measurements of the samples. 'IMR' represent Institute of Mineral Resources, Chinese Academy of Geological Sciences; 'CUG' represent China University of Geosciences

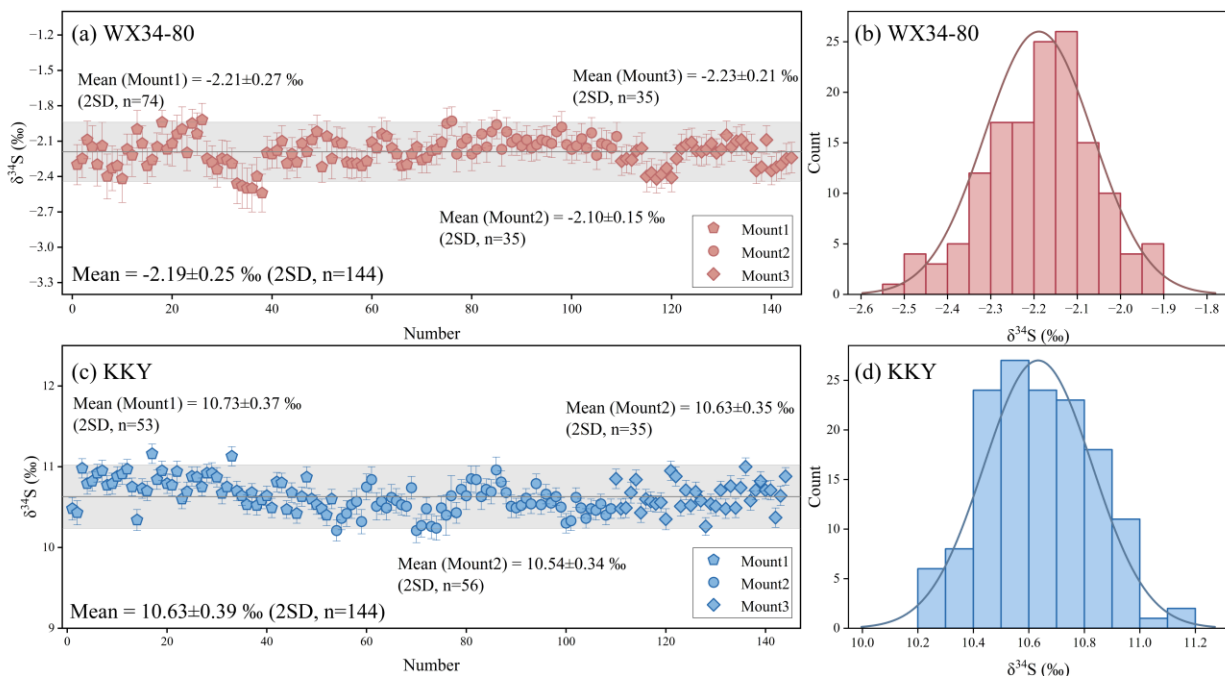


Fig. 4 Statistics of $\delta^{34}\text{S}$ values of WX34-80 and KKY from different epoxy mounts. (a), (c) : $\delta^{34}\text{S}$ values determined by LA-MC-ICP-MS. Range bars represent internal precision (2s) and shaded areas indicating external precision for repeated measurements. (b), (d) : frequency histograms and probability density curves.

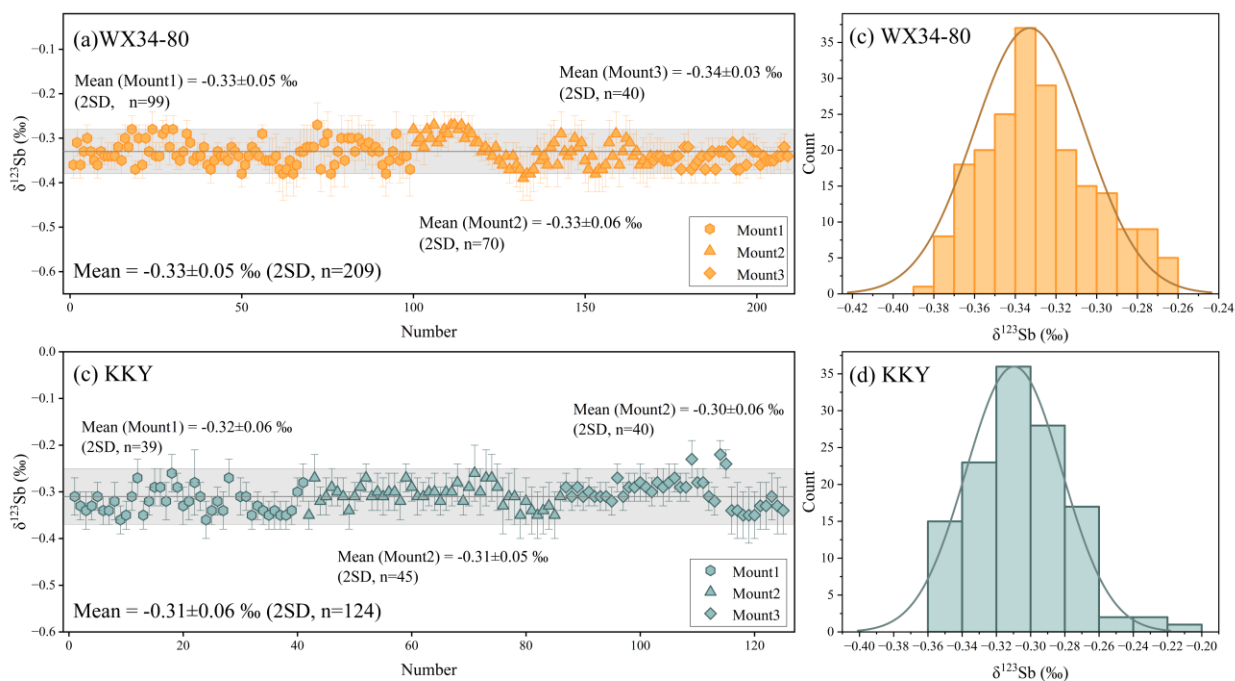


Fig. 5 Statistics of $\delta^{123}\text{Sb}$ values of WX34-80 and KKY from different epoxy mounts. (a), (c) : $\delta^{123}\text{Sb}$ values determined by LA-MC-ICP-MS. Range bars represent internal precision (2 s) and shaded areas indicating external precision for repeated measurements. (b), (d): frequency histograms and probability density curves.

Table 2. Kolmogorov-Smirnov test of the LA-MC-ICP-MS results

Name	Number	Type	Statistic (D)	P
WX34-80	144	$\delta^{34}\text{S}$	0.08	0.29
	209	$\delta^{123}\text{Sb}$	0.07	0.22
KKY	144	$\delta^{34}\text{S}$	0.06	0.52
	124	$\delta^{123}\text{Sb}$	0.07	0.65

Table 3. Summary of S and Sb isotopic compositions for WX34-80, KKY, and the previously published reference materials

Name	Source	$\delta^{34}\text{S}_{\text{VCDT}}(\text{‰})$	$\delta^{123}\text{Sb}_{\text{SpX}}(\text{‰})$	Method	Reference
BJ-Snt	natural	$-0.71 \pm 0.32\text{‰}$ (2SD)	/	IRMS	Dai <i>et al.</i> ³³
		$-0.78 \pm 0.34\text{‰}$ (2SD)	/	LA-MC-ICP-MS	Dai <i>et al.</i> ³³
		/	$0.14 \pm 0.05\text{‰}$ (2SD, n = 2)	SN-MC-ICP-MS	This study
		/	$0.14 \pm 0.04\text{‰}$ (2SD, n=45)	LA-MC-ICP-MS	This study
YS14	synthetic	/	$-2.66 \pm 0.20\text{‰}$ (2SD, n=5)	LA-MC-ICP-MS	Dai <i>et al.</i> ³³
DC	natural	/	$0.02 \pm 0.04\text{‰}$ (2SD)	SN-MC-ICP-MS	Wang <i>et al.</i> ³⁴
		/	$0.04 \pm 0.07\text{‰}$ (2SD)	LA-MC-ICP-MS	Wang <i>et al.</i> ³⁴
		$5.57 \pm 0.22\text{‰}$ (2SD, n=26)	/	LA-MC-ICP-MS	This study
BJS	natural	/	$-0.37 \pm 0.05\text{‰}$ (2SD)	SN-MC-ICP-MS	Wang <i>et al.</i> ³⁴
		/	$-0.39 \pm 0.06\text{‰}$ (2SD)	LA-MC-ICP-MS	Wang <i>et al.</i> ³⁴
		$6.26 \pm 0.19\text{‰}$ (2SD, n = 26)	$-0.34 \pm 0.05\text{‰}$ (2SD, n = 30)	LA-MC-ICP-MS	This study
SC	synthetic	/	$-0.189 \pm 0.031\text{‰}$ (n=20)	SN-MC-ICP-MS	Kaufmann <i>et al.</i> ³⁹
MAC	natural	/	$0.645 \pm 0.029\text{‰}$ (n=12)	SN-MC-ICP-MS	Kaufmann <i>et al.</i> ³⁹
MET	synthetic	/	$0.192 \pm 0.058\text{‰}$ (n=18)	SN-MC-ICP-MS	Kaufmann <i>et al.</i> ³⁹
WX34-80	natural	$-2.17 \pm 0.29\text{‰}$ (2SD, n = 18)	/	IRMS	This study
		/	$-0.33 \pm 0.07\text{‰}$ (2SD, n = 8)	SN-MC-ICP-MS	This study
		$-2.19 \pm 0.25\text{‰}$ (2SD, n = 144)	$-0.33 \pm 0.05\text{‰}$ (2SD, n=209)	LA-MC-ICP-MS	This study
KKY	natural	$10.63 \pm 0.38\text{‰}$ (2SD, n = 18)	/	IRMS	This study
		/	$-0.29 \pm 0.05\text{‰}$ (2SD, n = 8)	SN-MC-ICP-MS	This study
		$10.63 \pm 0.39\text{‰}$ (2SD, n = 144)	$-0.31 \pm 0.06\text{‰}$ (2SD, n=124)	LA-MC-ICP-MS	This study

LA-MC-ICP-MS Sb isotope measurement. Following the same random spot approach used for sulfur isotopes, in situ antimony isotope analysis was conducted on stibnite from the sample mounts. For sample WX34-80, a total of 209 analytical spots were measured. These were distributed across three mounts: 99 spots on mount 1, 70 on mount 2, and 40 on mount 3, yielding average $\delta^{123}\text{Sb}$ values of $-0.33 \pm 0.05\text{‰}$ (2SD, n = 99), $-0.33 \pm 0.06\text{‰}$ (2SD, n = 70), and $-0.34 \pm 0.03\text{‰}$ (2SD, n = 40), respectively, and yielding an overall average $\delta^{123}\text{Sb}$ value of $-0.33 \pm 0.05\text{‰}$ (2SD, n = 209) (Fig. 5a–b). For sample KKY, 124 analytical spots were obtained, 39 spots on mount 1, 45 spots on mount 2, and 40 spots on mount 3. The corresponding average $\delta^{123}\text{Sb}$ values were $-0.32 \pm 0.06\text{‰}$ (2SD, n = 39), $-0.31 \pm 0.05\text{‰}$ (2SD, n = 45), and $-0.30 \pm 0.06\text{‰}$ (2SD, n = 40), respectively, yielding an overall average $\delta^{123}\text{Sb}$ value of $-0.31 \pm 0.06\text{‰}$ (2SD, n = 124) (Fig. 5c–d). The mean $\delta^{123}\text{Sb}$ values from in situ analysis were consistent, within 2SD uncertainty, with those obtained by solution-based SN-MC-ICP-MS for the respective samples ($-0.33 \pm 0.07\text{‰}$ for WX34-80 and $-0.29 \pm 0.05\text{‰}$ for KKY).

Kolmogorov–Smirnov tests indicated that the in situ S and Sb isotopic compositions of stibnite samples WX34-80 and KKY

were consistent with a normally distributed (Gaussian) population (Table 2). The twice standard deviation (S: 0.25‰ for WX34-80 and 0.39‰ for KKY; Sb: 0.05‰ for WX34-80 and 0.06‰ for KKY), obtained from many analytical spots, indicated good S and Sb isotopic homogeneity of both samples at the 30 μm sampling scale.

Comparison with reported reference materials. Table 3 summarizes the previously published reference materials, along with the two newly characterized reference materials developed in this study for in situ S and Sb isotope analyses of stibnite. They are mainly divided into two categories: synthetic materials, such as YS14 for in situ S isotope analysis and SC and MET for Sb isotope analysis. These types of samples are primarily employed for fs-LA-MC-ICP-MS analyses, where matrix effects are considered negligible. However, potential matrix effects may still exist when these materials are applied to ns-LA-MC-ICP-MS analyses. The other category consists of matrix-matched natural materials, including natural stibnite reference materials for S (BJ-Snt) and Sb isotope analyses (MAC, DC, and BJS). WX34-80 and KKY exhibited the lowest and the highest $\delta^{34}\text{S}$ values, respectively, thereby expanding the range of sulfur isotopic compositions

available for stibnite reference materials. These two reference materials exhibited high homogeneity in their S and Sb isotopic compositions, which were comparable to those of existing reference materials. This mitigated the shortage of sulfur and antimony isotope reference materials. To facilitate broader application of the published reference materials, we supplemented the missing isotope compositions for the existing standards. We performed in situ sulfur isotope analysis on the stibnite reference materials DC and BJS, yielding $\delta^{34}\text{S}$ values of $5.57 \pm 0.22\text{‰}$ (2SD, $n = 26$) and $6.26 \pm 0.19\text{‰}$ (2SD, $n = 26$), respectively. Additionally, in situ antimony isotope analysis of the reference material BJ-Snt yielded a $\delta^{123}\text{Sb}$ value of $0.14 \pm 0.04\text{‰}$ (2SD, $n = 45$).

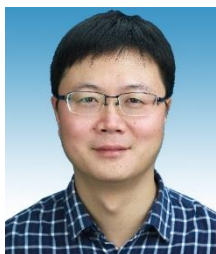
CONCLUSION

This study employed multiple analytical techniques to determine the S and Sb isotopic compositions of stibnite the samples WX34-80 and KKY. Results from both bulk-rock and micro-scale analyses indicated that both samples exhibited homogeneous S and Sb isotopic compositions at both the hand-specimen scale and the micro-beam scale (30 μm). The samples had simple matrix compositions, making them suitable reference materials. Gas-source IRMS yielded $\delta^{34}\text{S}_{\text{V-CDT}}$ values of $-2.17 \pm 0.29\text{‰}$ (2SD, $n = 18$) for WX34-80 and $10.63 \pm 0.38\text{‰}$ (2SD, $n = 18$) for KKY, while SN-MC-ICP-MS provided $\delta^{123}\text{Sb}_{\text{Spex}}$ values of $-0.33 \pm 0.07\text{‰}$ (2SD, $n = 8$) and $-0.29 \pm 0.05\text{‰}$ (2SD, $n = 8$), respectively, which can be considered the recommended values. Both samples are available in quantities exceeding 1 kg for further research purposes, and interested laboratories may contact the corresponding authors to request. Furthermore, this study supplemented the published stibnite reference material BJ-Snt with additional Sb isotope data, and provided additional S isotope data for samples DC and BJS, to facilitate wider application of these reference materials.

ASSOCIATED CONTENT

The supporting information (Tables S1) is available at <https://www.at-spectrosc.com>

AUTHOR INFORMATION



Kejun Hou received his PhD in 2014 from the China University of Geosciences (Beijing). He is a research professor of geochemistry at the Institute of Mineral Resources, CAGS. His research focuses on in situ isotopic analysis using laser ablation multi-collector ICP-MS and its application to ore deposits. Hou Kejun has published over 200 papers as an author or

co-author on isotopic analysis and its applications in ore deposit geology. He currently serves as a guest editor of *Atomic Spectroscopy*.

Corresponding Author

* K. J. Hou

Email address: kejunhou@126.com

Notes

The authors declare no competing financial interest.

ACKNOWLEDGMENTS

This project was supported by the National Natural Science Foundation of China (42273035) and the Basic Scientific Research Business Expenses of Central Public Welfare Research Institutes (JKYZD202314). We thank Dr. Zhihui Dai for providing the BJ-Snt sample, Dr. Chao Li for providing the DC and BJS samples, and the reviewers and editors for their valuable comments.

REFERENCES

1. X. J. Liu, S. Liu, and S. Y. Peng, *Western Resources*, 2018, **4**, 201-203.
<https://d.wanfangdata.com.cn/periodical/CiBQZXJpb2RyY2FsQ0hJU29scjkyMDI2MDMwNjE2NTI1NnI0eGJ6eTlwMTgwNDA5MhoIN2VIZ3VjeXo%6D>
2. Y. J. Zhou, J. W. Li, G. S. Wang, Y. Xia, and N. P. Qiu, *China Mining Magazine*, 2014, **23(10)**, 13-16.
<https://www.cnki.com.cn/Article/CJFDTOTAL-ZGKA201410005.htm>
3. Q. J. Wu, Z. F. Lv, and J. C. Cao, *Multipurpose Utilization of Mineral Resources*, 2022, **43**, 77-82.
<http://www.kczhly.com/en/article/doi/10.3969/j.issn.1000-6532.2022.05.014>
4. H. G. Dill, F. Melcher, and R. Botz, *Ore Geol. Rev.*, 2008, **34**, 242-262. <https://doi.org/10.1016/j.oregeorev.2007.10.004>
5. R. Z. Hu, S. L. Fu, Y. Huang, M. F. Zhou, S. H. Fu, C. H. Zhao, Y. J. Wang, X. W. Bi, and J. F. Xiao, *J. Asian Earth Sci.*, 2017, **137**, 9-34. <https://doi.org/10.1016/j.jseaes.2016.10.016>
6. H. Li, Q. H. Wu, N. J. Evans, Z. K. Zhou, H. Kong, X. S. Xi, and Z. W. Lin, *Gondwana Res.*, 2018, **55**, 112-134.
<https://doi.org/10.1016/j.gr.2017.11.010>
7. S. L. Fu, R. Z. Hu, R. S. Yin, J. Yan, X. F. Mi, Z. C. Song, and N. A. Sullivan, *Miner. Deposita.*, 2020, **55**, 1353-1364.
<https://doi.org/10.1007/s00126-019-00940-1>
8. S. L. Fu, R. Z. Hu, X. W. Bi, N. A. Sullivan, and J. Yan, *Appl. Geochem.*, 2020, **118**, 104637.
<https://doi.org/10.1016/j.apgeochem.2020.104637>
9. X. Y. Jiang, Beijing: China University of Geosciences., Master's Thesis, 2023.
https://kns.cnki.net/kcms2/article/abstract?v=zO3wb1M9ekwW603sF4WDPbHoTJ2IvHb4jMCRmJawbN7yJHHeErzjob5CY5M_KFj

- 9nG5GDVsT5fk7O94eTFXEnYxGR7WQ8BgPS94KBLzRqPO
NzyczCuU-LtSZOM-
Ki8tT9xC6gb0vequJaazl7fKfY6KQoQTm2DSPOGDqa_tVq5m411
c1-U1O-MPw=&uniplatform=NZKPT&language=CHS
10. P. Koděra, R. Mathur, D. G. Zhai, R. Milovský, P. Bačo, and J. Majzlan, *Miner. Deposita.*, 2025, **60**, 1141-1157. <https://doi.org/10.1007/s00126-024-01333-9>
 11. Z. Z. Du, X. X. Gu, G. Q. Li, Y. M. Zhang, W. B. Cheng, L. B. Jiang, and X. G. Zhang, *Geoscience*, 2011, **25**, 853-860. https://xueshu.baidu.com/usercenter/paper/show?paperid=526906fcb88eac5fc2a0c79ec2ac055a&site=xueshu_se
 12. M. O. Aung, X. B. Lv, Z. Khin, H. Than, B. K. Sun, and M. A. A. Munir, *Minerals*, 2020, **10**, 296. <https://doi.org/10.3390/min10040296>
 13. H. Li, H. Kong, B. Y. Guo, L. Soh Tamehe, Q. Zhang, Q. H. Wu, and X. S. Xi, *Ore Geol. Rev.*, 2020, **126**, 103759. <https://doi.org/10.1016/j.oregeorev.2020.103759>
 14. B. L. Li, L. Q. Wang, X. G. Zhang, D. J. Pingcuo, T. Gao, and Y. Wang, *Acta Geosci. Sin.*, 2022, **43**, 202-210. <https://doi.org/10.3975/cagsb.2021.041501>
 15. Y. Li, C. H. Wang, Y. B. Li, Y. Sun, M. Puchi, X. D. Zhang, G. Lamu, and Z. Yang, *Front. Earth Sci.*, 2023, **10**, 1033124. <https://doi.org/10.3389/feart.2022.1033124>
 16. X. Y. Lin, M. S. Lin, J. F. Wu, Y. G. Yi, K. Xu, and J. Xu, *Journal of Chengdu University of Technology (Science & Technology Edition)*, 2025, **52**, 270-284. <https://doi.org/10.12474/cdlgzrxx.2024010403>
 17. O. Rouxel, J. Ludden, and Y. Fouquet, *Chem. Geol.*, 2003, **200**, 25-40. [https://doi.org/10.1016/S0009-2541\(03\)00121-9](https://doi.org/10.1016/S0009-2541(03)00121-9)
 18. S. Asaoka, Y. Takahashi, Y. Araki, and M. Tanimizu, *Anal. Sci.*, 2011, **27**, 25-28. <https://doi.org/10.2116/analsci.27.25>
 19. M. Tanimizu, Y. Araki, S. Asaoka, and Y. Takahashi, *Geochem. J.*, 2011, **45**, 27-32. <https://doi.org/10.2343/GEOCHEM.J.1.0088>
 20. L. Lobo, V. Devulder, P. Degryse, and F. Vanhaecke, *J. Anal. At. Spectrom.*, 2012, **27**, 1304-1310. <https://doi.org/10.1039/C2JA30062A>
 21. L. Lobo, P. Degryse, A. Shortland, F. Vanhaecke, *J. Anal. At. Spectrom.*, 2013, **28**, 1213-1219. <https://doi.org/10.1039/C3JA50018G>
 22. L. Lobo, P. Degryse, A. Shortland, K. Eremin, and F. Vanhaecke, *J. Anal. At. Spectrom.*, 2014, **29**, 58-64. <https://doi.org/10.1039/C3JA50303H>
 23. P. Degryse, L. Lobo, A. Shortland, F. Vanhaecke, A. Blomme, J. Painter, D. Gimeno, K. Eremin, J. Greene, S. Kirk, and M. Walton, *J. Archaeol. Sci.*, 2015, **62**, 153-60. <https://doi.org/10.1016/j.jas.2015.08.004>
 24. G. Y. Sun, Y. J. Wu, X. B. Feng, X. Wu, X. Y. Li, Q. W. Deng, F. Y. Wang, and X. W. Fu, *Chem. Geol.*, 2021, **582**, 120459. <https://doi.org/10.1016/j.chemgeo.2021.120459>
 25. J. Liao, D. C. Tan, H. B. Qin, Q. Han, E. G. Liu, J. A. Chen, Z. P. Ning, and S. H. Li, *J. Hazard. Mater.*, 2023, **454**, 131553. <https://doi.org/10.1016/j.jhazmat.2023.131553>
 26. X. Y. Li, G. Y. Sun, Y. J. Wu, M. Y. Zhou, Z. G. Li, X. Y. Bi, J. H. Huang, and X. B. Feng, *Int. J. Coal Geol.*, 2023, **265**, 104165. <https://doi.org/10.1016/j.coal.2022.104165>
 27. P. Degryse, L. Lobo, A. Shortland, F. Vanhaecke, A. Blomme, J. Painter, D. Gimeno, K. Eremin, J. Greene, S. Kirk, and M. Walton, *J. Archaeol. Sci.*, 2015, **62**, 153-160. <https://doi.org/10.1016/j.jas.2015.08.004>
 28. T. P. Ding, R. M. Bai, Y. H. Li, D. F. Wan, X. Q. Zou, and Q. L. Zhang, *Sci. China Ser. D-Earth Sci.*, 1999, **42**, 45-51. <https://doi.org/10.1007/BF02878497>
 29. S. A. Studley, E. M. Ripley, E. R. Elswick, M. J. Dorais, J. Fong, D. Finkelstein, and L. M. Pratt, *Chem. Geol.*, 2002, **192**, 141-148. [https://doi.org/10.1016/S0009-2541\(02\)00162-6](https://doi.org/10.1016/S0009-2541(02)00162-6)
 30. P. R. Craddock, O. J. Rouxel, L. A. Ball, and W. Bach, *Chem. Geol.*, 2008, **253**, 102-113. <https://doi.org/10.1016/j.chemgeo.2008.04.017>
 31. N. Lv, Z. A. Bao, K. Y. Chen, C. L. Zong, Y. Zhang, and H. L. Yuan, *Geostand. Geoanal. Res.*, 2022, **46**, 451-463. <https://doi.org/10.1111/ggr.12440>
 32. S. Y. Jiang, W. Chen, K. D. Zhao, D. Zhang, J. Lu, H. D. Zhao, *Journal of Chinese Mass Spectrometry Society*, 2021, **42**, 623-640. <https://zpxb.xml-journal.net/article/pdf/preview/zpxb-2996>
 33. Z. H. Dai, S. L. Fu, Y. F. Liu, Y. M. Meng, Z. A. Bao, K. J. Hou, and T. G. Lan, *J. Anal. At. Spectrom.*, 2024, **39**, 216-226. <https://doi.org/10.1039/D3JA00308F>
 34. W. Wang, C. Li, Z. Bo, J. H. Zhang, P. Y. Yu, H. Y. Ren, X. W. Li, L. M. Zhou, and W. J. Qu, *Atom. Spectrosc.*, 2024, **45**, 33-43. <https://doi.org/10.46770/AS.2024.013>
 35. X. F. Song, J. Q. Lai, J. W. Xu, X. H. Liu, B. Li, H. S. He, Y. H. Wang, J. Shi, C. F. Wang, and C. H. Wen, *Minerals*, 2022, **12**, 1407. <https://doi.org/10.3390/min12111407>
 36. W. Zhang, Y. S. Liu, and Z. C. Hu, *Mineralogy, Petrology and Geochemistry Communications*, 2018, **37**, 812-826. <https://www.sciengine.com/BMPG/doi/10.19658/j.issn.1007-2802.2018.37.111>
 37. Y. S. Liu, Z. C. Hu, M. Li, and S. Gao, *Chin Sci Bull.*, 2013, **58**, 3863-3878. <https://doi.org/10.1007/s11434-013-5901-4>
 38. K. J. Hou and Y. H. Li, *Miner. Deposits*, 2010, **55**, 2207-2213. <https://doi.org/10.1007/s11434-010-4064-9>
 39. A. B. Kaufmann, M. Lazarov, S. Kiefer, J. Majzlan, and S. Weyer, *J. Anal. At. Spectrom.*, 2021, **36**, 1554-1567. <https://doi.org/10.1039/D1JA00089F>
 40. L. Chen, H. L. Yuan, K. Y. Chen, Z. A. Bao, L. M. Zhu, and P. Liang, *J. Asian Earth Sci.*, 2019, **176**, 325-336. <https://doi.org/10.1016/j.jseas.2019.02.017>
 41. J. L. Fu, Z. C. Hu, J. W. Li, L. Yang, W. Zhang, Y. S. Liu, Q. L. Li, K. Q. Zong, and S. H. Hu, *J. Anal. At. Spectrom.*, 2017, **32**, 2341-2351. <https://doi.org/10.1039/C7JA00282C>
 42. J. Lin, Y. S. Liu, Z. C. Hu, W. Chen, C. X. Zhang, K. D. Zhao, and X. Y. Jin, *J. Anal. At. Spectrom.*, 2019, **34**, 1145-1153. <https://doi.org/10.1039/C9JA00013E>
 43. W. Zhang, Y. Hu, S. S. Lu, Z. C. Hu, X. L. Zeng, S. J. Yang, and Z. Y. Liu, *Earth Science*, 2024, **49**, 3890-3903. <http://www.earth-science.net/article/doi/10.3799/dqkx.2024.097>
 44. Y. T. Feng, Wuhan: China University of Geosciences., Doctoral thesis, 2022. <https://cdmd.cnki.com.cn/Article/CDMD-10491-1023827020.htm>
 45. S. Wang, Y. Y. Gao, J. Wang, and T. X. Ren, *Journal of Chinese Mass Spectrometry Society*, 2021, **42**, 641-655. <https://zpxb.xml-journal.net/article/pdf/preview/zpxb-2997>
 46. X. X. Gu, Y. M. Zhang, O. Schulz, F. Vavtar, J. M. Liu, M. H. Zheng, and L. Zheng, *J. Asian Earth Sci.*, 2012, **57**, 54-75. <https://doi.org/10.1016/j.jseas.2012.06.006>
 47. Z. K. Zhou, H. Li, K. Yonezu, A. Imai, and T. Tindell, *J. Geochem. Explor.*, 2023, **247**, 107177. <https://doi.org/10.1016/j.gexplo.2023.107177>
 48. P. Zhang, P. K. Tang, and A. Q. Chen, *Mineral Exploration*, 2019, **10**, 530-536, 1674-7801.

- http://www.kckc.org.cn/ch/reader/view_abstract.aspx?file_no=20190316&flag=1
49. L. L. Jia, T. Dai, C. Z. Xi, and D. X. Zhang, *Chem. Eng. Trans.*, 2017, **62**, 475-480. <https://doi.org/10.3303/CET1762080>
 50. S. Y. Yang, S. Y. Jiang, Q. Mao, Z. Y. Chen, C. Rao, X. L. Li, W. C. Li, W. Q. Yang, P. L. He, and X. Li, *Atom. Spectrosc.*, 2022, **43**, 186-200. <https://doi.org/10.46770/AS.2021.912>
 51. Y. S. Liu, Z. C. Hu, S. Gao, D. Günther, J. Xu, C. G. Gao, and H. H. Chen, *Chem. Geol.*, 2008, **257**, 34-43. <https://doi.org/10.1016/j.chemgeo.2008.08.004>
 52. B. Fry, S. R. Silva, C. Kendall, and R. Anderson, *Rapid Commun. Mass Spectrom.*, 2002, **16**, 854-858. <https://doi.org/10.1002/rcm.651>
 53. D. G. Zhai, R. Mathur, S. G. Liu, J. J. Liu, L. Godfrey, K. X. Wang, J. W. Xu, and J. Vervoort, *Geochim. Cosmochim. Acta.*, 2021, **306**, 84-97. <https://doi.org/10.1016/j.gca.2021.05.03>
 54. Y. Fang, K. Y. Chen, Z. A. Bao, C. L. Zong, H. L. Yuan, and N. Lv, *Anal. Chem.*, 2022, **94**, 16746-16751. <https://doi.org/10.1021/acs.analchem.2c03420>
 55. S. Y. Li, Y. L. Deng, H. T. Zheng, X. Liu, P. D. Tang, J. W. Zhou, and Z. L. Zhu, *J. Anal. At. Spectrom.*, 2021, **36**, 157-164. <https://doi.org/10.1039/D0JA00367K>
 56. J. F. Liu, J. B. Chen, T. Zhang, Y. N. Wang, W. Yuan, Y. C. Lang, C. L. Tu, L. Z. Liu and J.-L. Birck, *J. Anal. At. Spectrom.*, 2020, **35**, 1360-1367. <https://doi.org/10.1039/D0JA00136H>
 57. X. Y. Liu, L. Chen, F. D. Zhao, F. Huang, Q. L. Li, H. M. Yu, and X. H. Li, *J. Anal. At. Spectrom.*, 2026, **41**, 112-120. <https://doi.org/10.1039/D5JA00310E>
 58. L. H. Jia, Q. Mao, B. Su, S. T. Wu, L. L. Huang, J. Y. Yuan, D. Zhang, and Y. Chen, *Minerals*, 2021, **11**, 1321. <https://doi.org/10.3390/min11121321>
-